Journal of Geophysical Research: Solid Earth

Supporting Information for

Quantifying magma overpressure beneath a submarine caldera: A mechanical modeling approach to tsunamigenic trapdoor faulting near Kita-Ioto Island, Japan

Osamu Sandanbata[1,2†], and Tatsuhiko Saito[1]

[1] National Research Institute for Earth Science and Disaster Resilience, Ibaraki, Japan.

[2] *Now at* Earthquake Research Institute, the University of Tokyo, Tokyo, Japan.

Contents of this file

Additional Supporting Information (Files uploaded separately)

Introduction

This Supporting Information contains supplementary figures, tables and texts. Supplementary Figures S1–S8 and Table S1 are mentioned in Main Text. In Supplementary Texts, we describe our moment tensor analysis (Text S1) and commutations of long-period seismic waveforms from our trapdoor faulting model (Text S2), which include Supplementary Figure S9. Data Set S1 contains the data of our source model shown in Figure 3 in Main Text.

Supplementary figures (mentioned in Main Text)

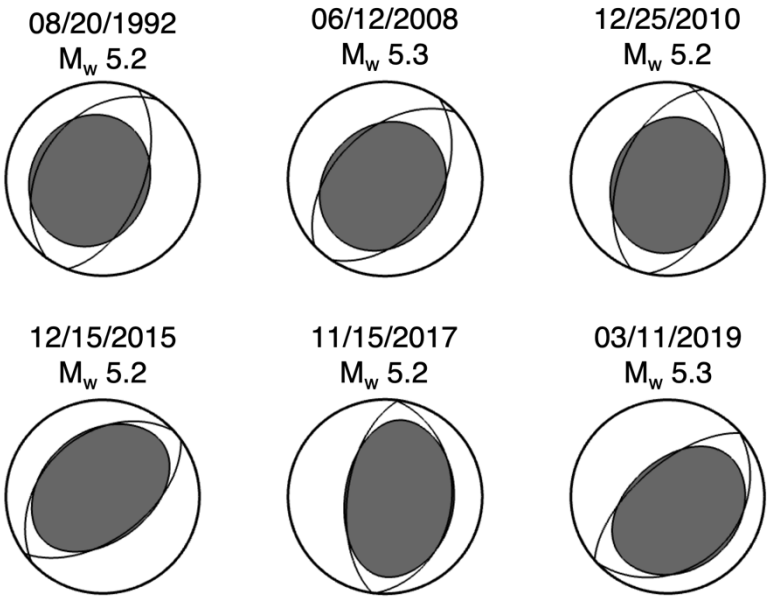

Figure S1. Moment tensors of vertical-T CLVD earthquakes repeating near Kita-Ioto Island, reported by the GCMT catalog (Ekström et al., 2012). The focal mechanisms are shown as projections of the lower focal hemisphere, and the orientation of the best double-couple solution is shown as thin lines.

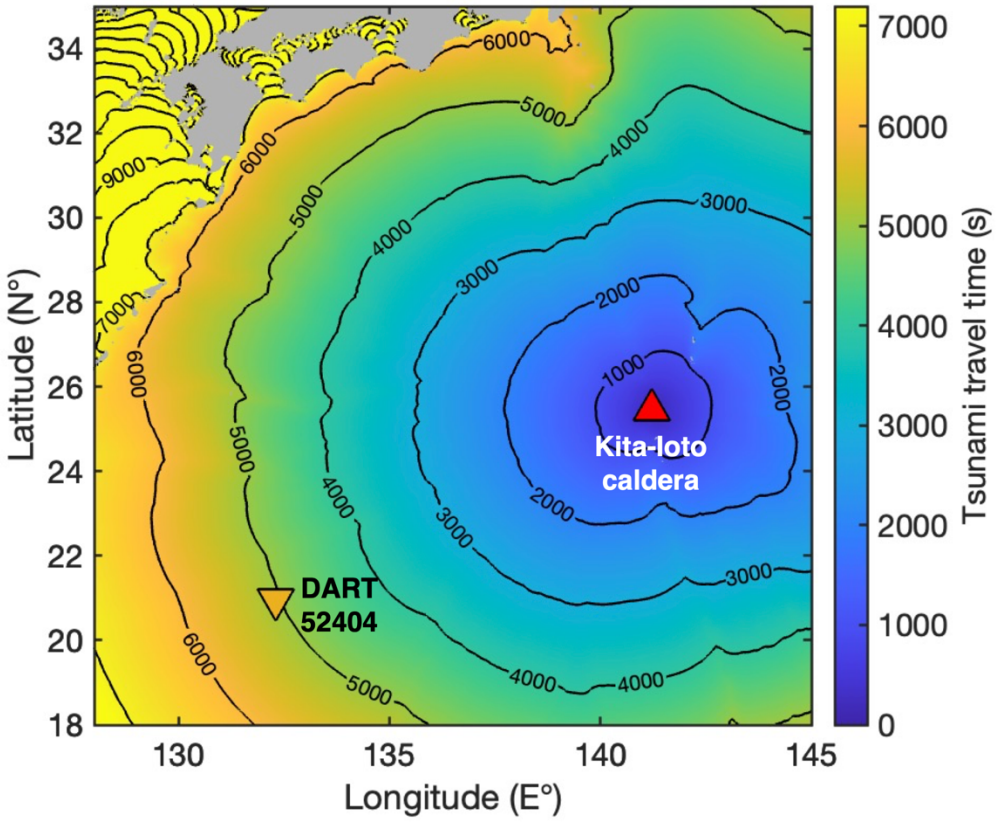

Figure S2. Tsunami travel time from the center of Kita-Ioto caldera (141.23E°, 25.45N°), computed by the Geoware TTT (Tsunami Travel Time) software. Red and orange triangles represent locations of Kita-Ioto caldera and DART 52404, respectively. The bathymetry data of JTOPO30 is used for the computation.

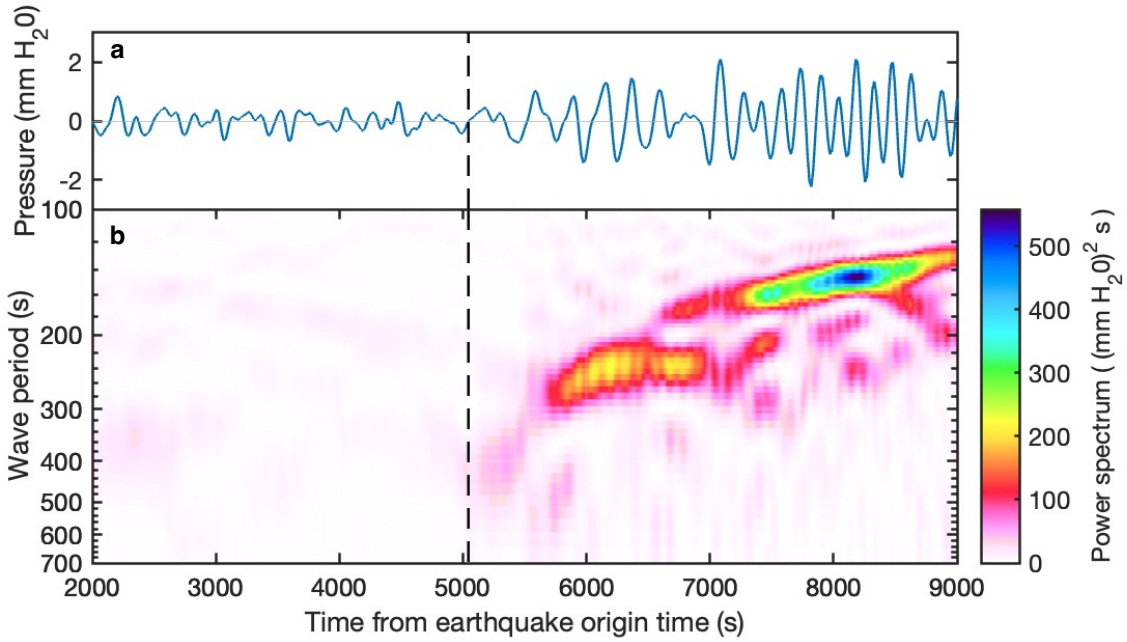

Figure S3. Spectrogram of the ocean-bottom-pressure (OBP) waveform of DART 52404 after the 2008 earthquake near Kita-Ioto caldera, at 13:10 on 12 June 2008. (**a**) The filtered OBP waveform (see Section 2 in Main Text for the filtering procedure). (**b**) Spectrogram of the OBP waveform. We obtain the spectral amplitude at successive time windows with a data length of 1,000 s and a time shift of 15 s.

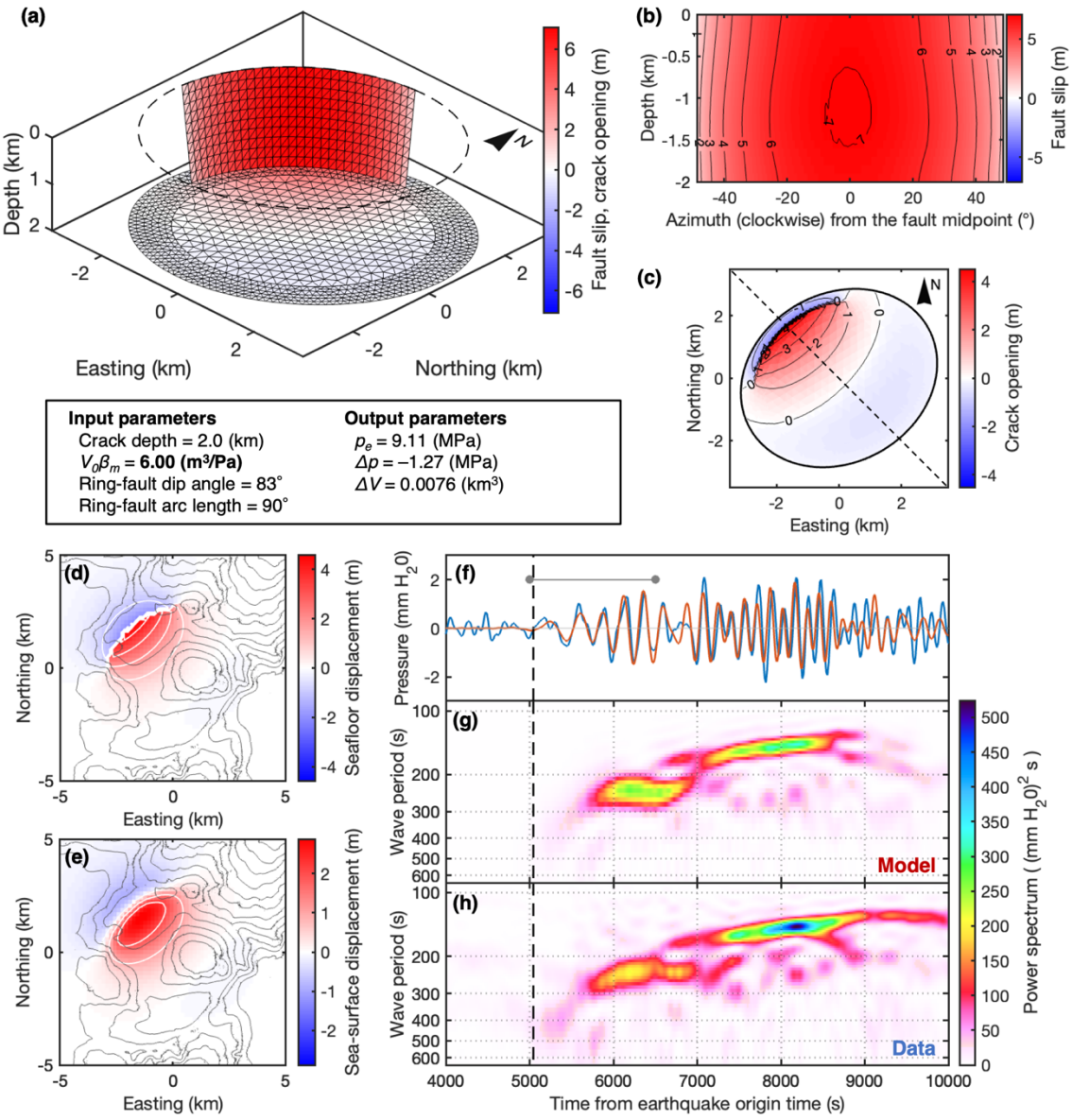

Figure S4. Same as Figure 3, but for a model with the product $V_0\beta_m$ of 6.00 m^3/Pa. See details in Section 6.1.3 of Main Text.

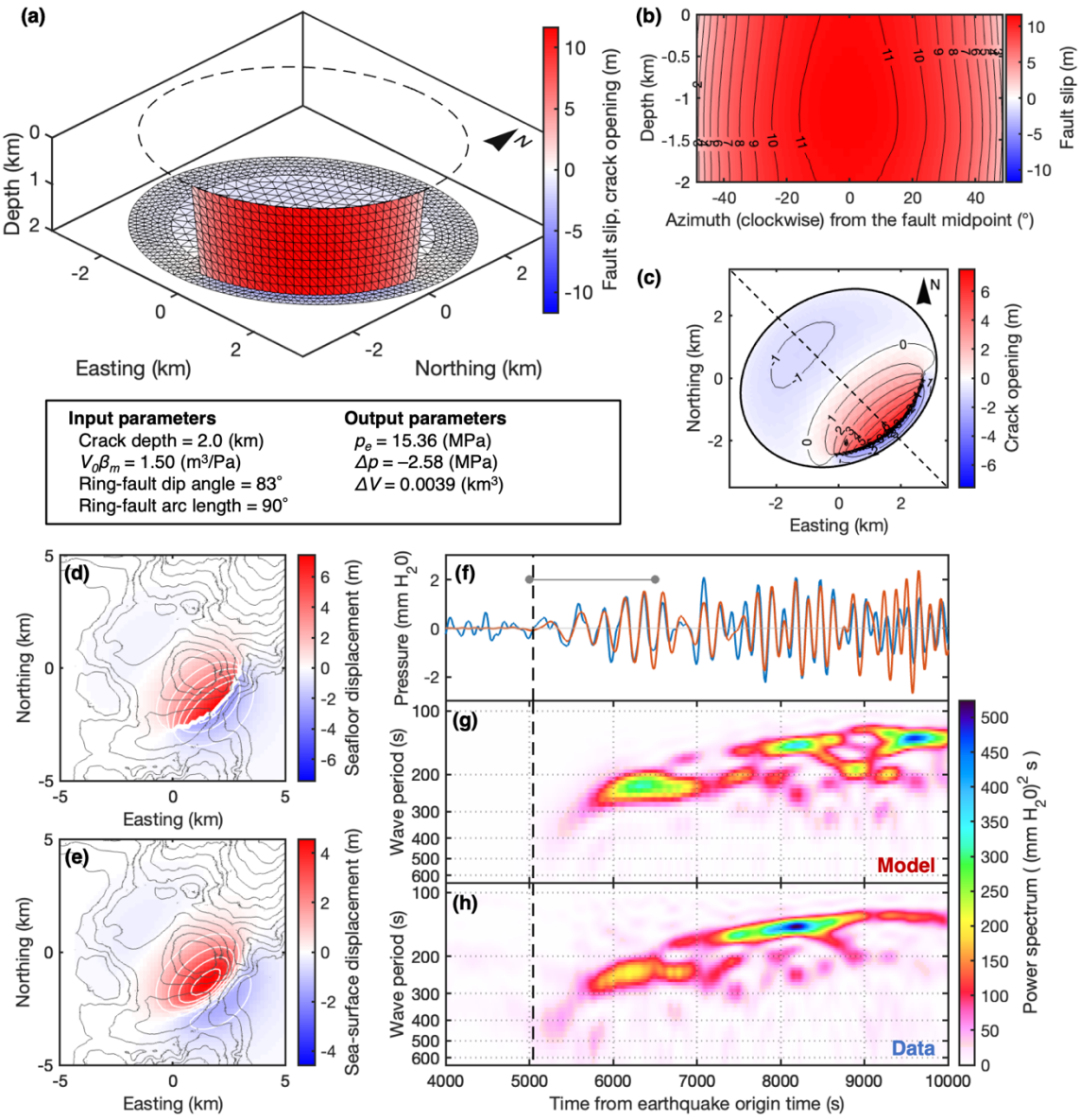

Figure S5. Same as Figure 3, but for a model with a ring fault on the SE side of the caldera. See details in Section 6.1.3 of Main Text.

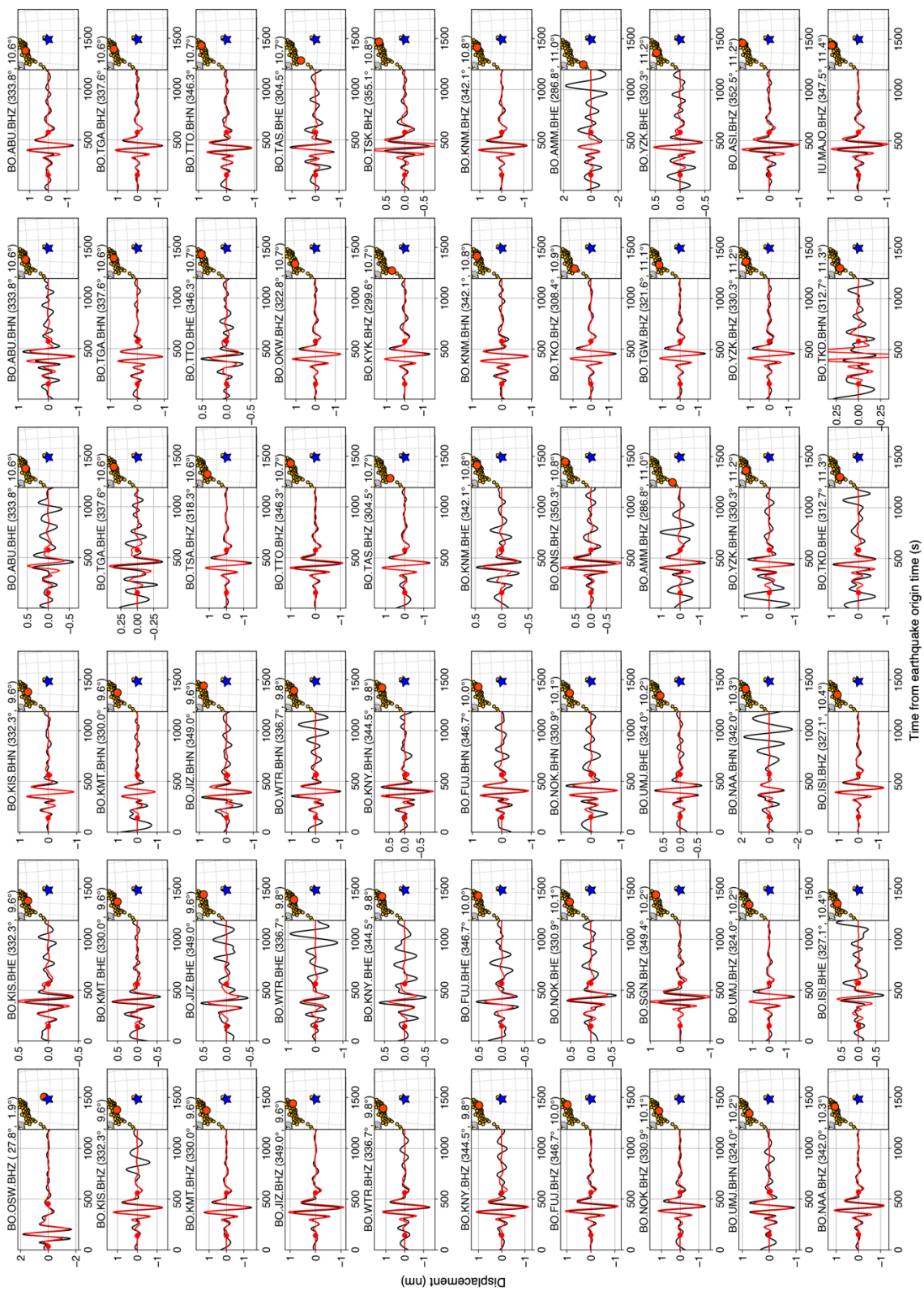

Figure S6. Same as Figure 8d, but for all the seismic stations.

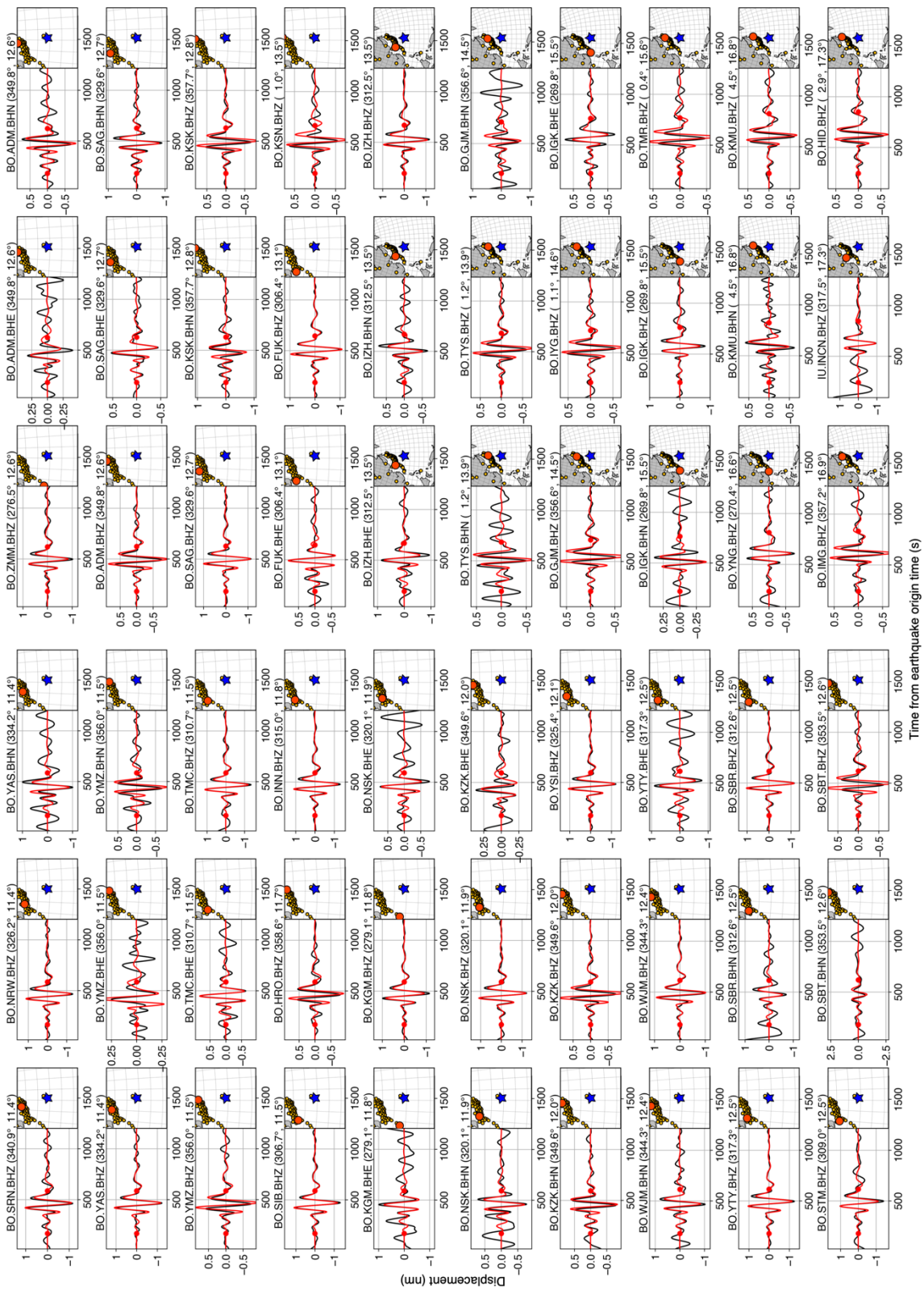

Figure S6. (continued)

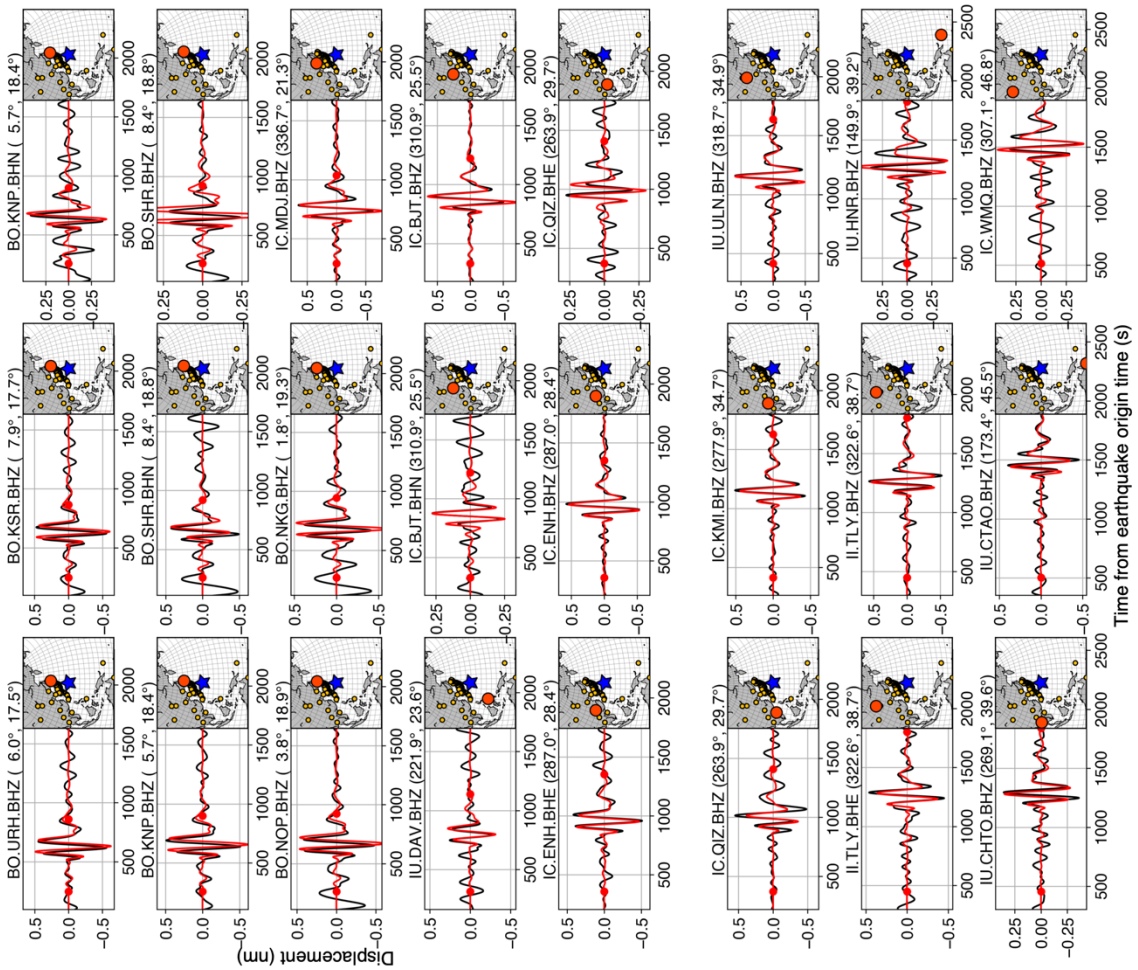

Figure S6. (continued)

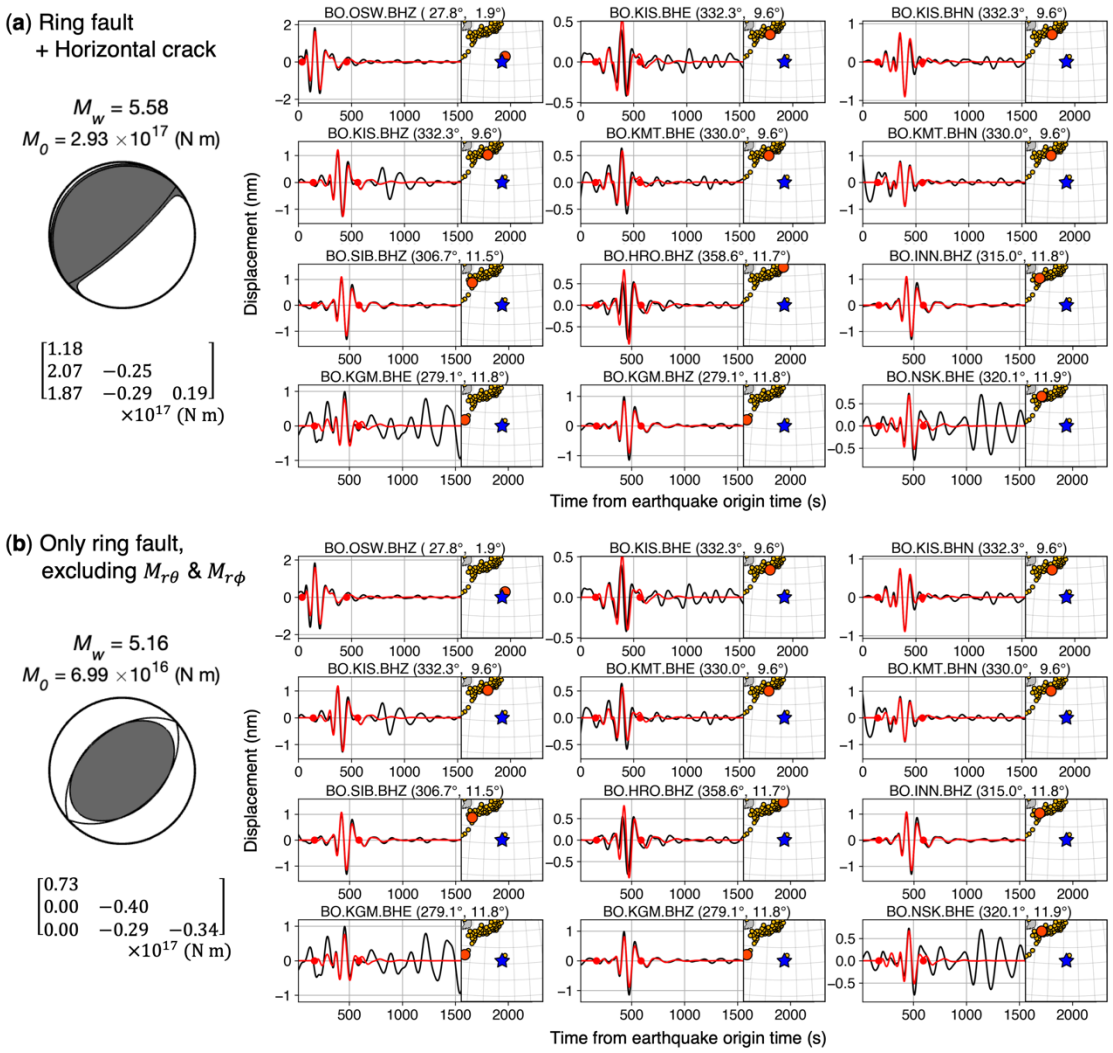

Figure S7. Moment tensors and synthetic seismograms of moment tensors of (**a**) our source model shown in Figure 3 ($\boldsymbol{M_T} = \boldsymbol{M_F} + \boldsymbol{M_C}$), and (**b**) only its ring fault part, excluding $M_{r\theta}$ and $M_{r\phi}$ components ($\boldsymbol{M_F}$, but with $M_{r\theta} = M_{r\phi} = 0$). See the caption of Figure 8d for descriptions of the seismograms. Note that the synthetic seismograms (red) in **a** and **b** are quite similar to each other, showing little contribution to the long-period seismic waves by the horizontal crack $\boldsymbol{M_C}$, and $M_{r\theta}$ and $M_{r\phi}$ components in $\boldsymbol{M_F}$.

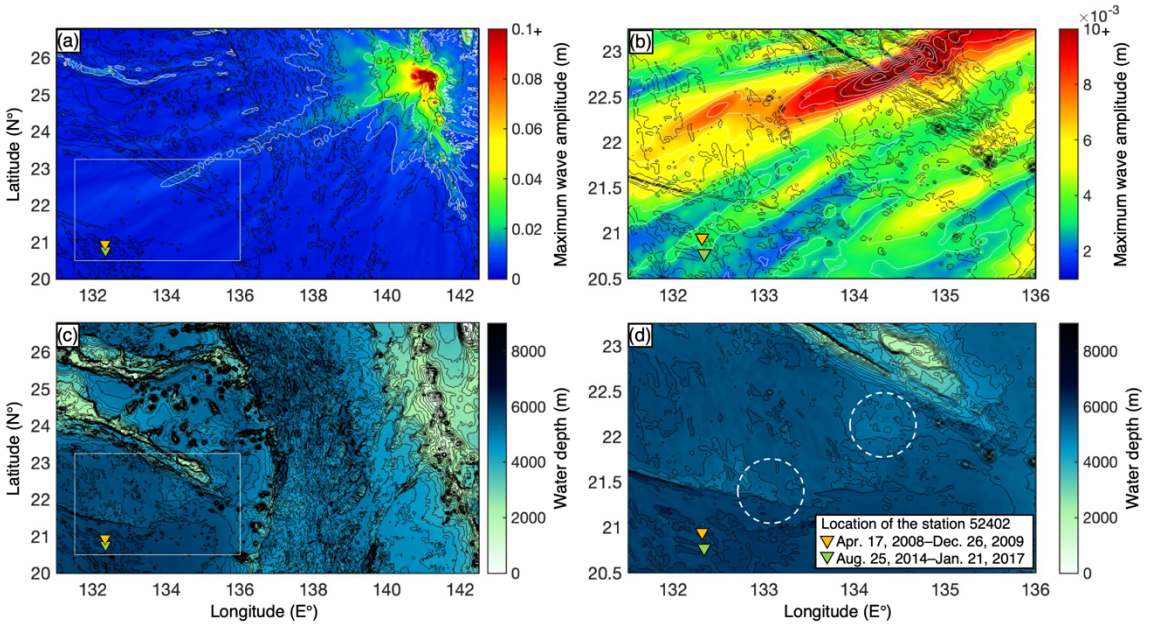

Figure S8. Focusing/defocusing effect by the bathymetry near the station 52404. (**a**–**b**) Maximum wave amplitude from the model shown in Figure 3. White and black lines represent contours of maximum wave amplitude (with intervals of 0.01 m in **a**, and of 0.001 m in **b**) and of water depth (with intervals of 1,000 m in **a**, and of 250 m in **b**). (**c**–**d**) Bathymetry. Black lines represent contours of water depth (with intervals of 250 m). Orange and green triangles represent locations of the station 52404 as of the 2008 and 2015 earthquakes, respectively. Note that the wave amplitude is expected to be larger at the station location as of 2008 than at the location as of 2015 (compare the maximum wave amplitudes at the two locations). This is because relatively shallow parts, represented by white dashed circles, cause focusing to the location as of 2008 and defocusing from the location as of 2015. This focusing/defocusing effect changes tsunami waveforms much at the two stations, although their locations were only ~20 km away.

Supplementary Tables (mentioned in Main Text)

Event #	Date (MM/DD/YYYY)	Time (HH:mm:ss)	Moment magnitude M_w	Depth (km)
1	08/20/1992	18:31:41.8	5.2	19.0
2	06/12/2008	13:10:13.5	5.3	12.0
3	12/25/2010	05:55:27.6	5.2	12.0
4	12/15/2015	00:20:36.5	5.2	12.0
5	11/15/2017	08:48:23.3	5.2	14.4
6	03/11/2019	09:33:51.7	5.3	25.53

Table S1. Earthquake information of vertical-T VCLVD earthquakes near Kita-Ioto Island, reported by the GCMT catalog (Ekström et al., 2012). The time is in UTC. Note that shallow source depths may not be determined accurately with long-period seismic data used for the catalog.

Supplementary texts

Text S1. Moment tensor analysis using long-period seismic waveform data

We analyze deviatoric moment tensor solutions of the Kita-Ioto caldera earthquakes reported in the GCMT catalog to extract information of the fault geometry of trapdoor faulting. Sandanbata et al. (2021) proposed a deviatoric moment tensor solution excluding $M_{r\theta}$ and $M_{r\phi}$, defined as a *resolvable moment tensor* $\boldsymbol{M}_{res}$, as a proxy of the source geometries of seismic events related to ring-faulting, including trapdoor faulting; the horizontal orientation of the nodal-axis (N-axis) of $\boldsymbol{M}_{res}$ coincides with the main fault orientation, while the ratio of the vertical-CLVD component to the double-couple component in $\boldsymbol{M}_{res}$ reflects the arc length of a ring-fault system.

To apply their method to the Kita-Ioto caldera earthquakes in 2008, we obtain $\boldsymbol{M}_{res}$ of the two events by adjusting $M_{r\theta}$ and $M_{r\phi}$ of their GCMT solution as zero (Figure S9a). $\boldsymbol{M}_{res}$ of the 2008 earthquake has an N-axis oriented in the NE–SW direction, and a dominant vertical-CLVD component (~85 %). Following the relationships between these parameters and the ring-fault geometry (Figure 4 in Sandanbata et al. [2021]), this $\boldsymbol{M}_{res}$ solution suggests that a ring fault ruptured by the earthquake was oriented in the NE-SW direction and with a ~135° arc length, if a circular ring fault system is assumed. Based on this estimation, we have assumed a ring fault with an arc length of 90°–180° on the NW or SE sides of the caldera in our analyses.

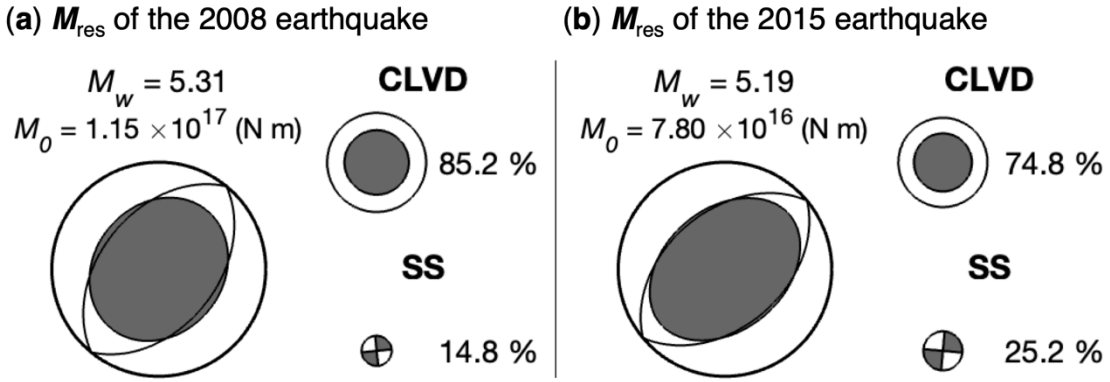

Figure S9. Resolvable moment tensors, obtained by excluding $\boldsymbol{M}_{r\theta}$ and $\boldsymbol{M}_{r\phi}$ from the GCMT solutions, of the Kita-Ioto caldera earthquakes on 12 June 2008 and 15 December 2015. The best double-couple solution is shown by thin curves. *CLVD* and *SS* represent the vertical-CLVD and vertical strike-slip components contained in the solutions, respectively, which were defined by Sandanbata et al. (2021).

For further investigation, we apply the method to the 2015 earthquake, to evaluate the similarity between the 2008 and 2015 earthquakes. Figure S9b shows that $\boldsymbol{M}_{res}$ of the 2015 earthquake contains a similar N-axis oriented in the NE-SW direction but with a less dominant vertical-CLVD component, compared to the 2008 earthquake. The N-axis similarly and the CLVD-ratio difference can be explained by assuming that the 2008 and

2015 earthquakes occurred along a ring fault on the same side of the caldera but a shorter fault ruptured during the 2015 earthquake. Thus, these analyses support our speculation of recurrent trapdoor faulting inferred from the tsunami data (see Section 6.4 in Main Text).

Text S2. Computing long-period seismic waveforms

For seismic validation of our model, we synthetize long-period (80–200 s) seismic waveforms at regional and global stations. We approximate our trapdoor faulting model, composed of a number of sub-faults and sub-cracks, as a point-source moment tensor, following the method of Sandanbata et al. (2022; 2023). We first calculate separately moment tensors of the ring fault ($\boldsymbol{M_F}$) and the horizontal crack ($\boldsymbol{M_C}$) by summing up moment tensors of a number of sub-faults and sub-cracks, respectively (pp. 695–699 in Aki & Richards, 1980; Kawakatsu & Yamamoto, 2015), where the Lamé's constants are 5 GPa. We then obtain a composite moment tensor of the trapdoor faulting model $\boldsymbol{M_T}$ by summing up the two moment tensors, or $\boldsymbol{M_T} = \boldsymbol{M_F} + \boldsymbol{M_C}$.

Assuming $\boldsymbol{M_T}$ as an initial condition, we compute seismic waveforms by using the W-phase package (Duputel et al., 2012; Hayes et al., 2009; Kanamori & Rivera, 2008). Seismic data of BH channels at stations within 1°–50° epicentral distance are downloaded from the F-net (National Research Institute for Earth Science and Disaster Resilience, 2019) and global seismic networks (network codes: IU, IC, and II). We remove the instrument response from the seismic data to obtain the displacement records. After data screening process to select seismic records with a good signal-to-noise ratio, we synthesize seismic waveforms at the stations by using the Green's function computed by the normal mode method (Takeuchi & Saito, 1972) with the 1-D Preliminary Reference Earth Model (PREM) (Dziewonski & Anderson, 1981), when we assume the centroid at the center of Kita-Ioto caldera (141.220°E, 25.452°N) and at a depth of 0.5 km in the crust. We apply a one-pass fourth-order band-pass Butterworth filter with corner frequencies of 0.005 and 0.0125 Hz (band-pass period = 80–200 s) to extract long-period seismic waveforms form both synthetic and observed seismic records.

We show the moment tensors ($\boldsymbol{M_T}$, $\boldsymbol{M_F}$, and $\boldsymbol{M_C}$) and compare the synthetic and observed seismic waveforms in representative records in Figure 8, as well as the waveforms at all the tested stations in Figure S6. Although there are slight mispredictions of waveform amplitude and phase in some records, possibly due to computation based on 1-D Earth model without lateral heterogeneity of the Earth structure, long-period seismograms at the stations covering wide azimuth are overall reproduced by our model, supporting plausibility of our model in terms of long-period seismic excitation.

Data Set S1. Dataset for our mechanical model of trapdoor faulting (separate file), including a model presented in Figure 3 in Main Text. This dataset is available from a repository, Zenodo (https://doi.org/10.5281/zenodo.8344070).

References

Aki, K., & Richards, P. G. (1980). *Quantitative seismology: theory and methods* (Vol. 842). Freeman San Francisco, CA.

Duputel, Z., Rivera, L., Kanamori, H., & Hayes, G. (2012). W phase source inversion for moderate to large earthquakes (1990–2010). *Geophysical Journal International*, *189*(2), 1125–1147. https://doi.org/10.1111/j.1365-246X.2012.05419.x

Dziewonski, A. M., & Anderson, D. L. (1981). Preliminary reference Earth model. *Physics of the Earth and Planetary Interiors*, *25*(4), 297–356. https://doi.org/10.1016/0031-9201(81)90046-7

Ekström, G., Nettles, M., & Dziewoński, A. M. (2012). The global CMT project 2004–2010: Centroid-moment tensors for 13,017 earthquakes. *Physics of the Earth and Planetary Interiors*, *200–201*, 1–9. https://doi.org/10.1016/j.pepi.2012.04.002

Hayes, G. P., Rivera, L., & Kanamori, H. (2009). Source Inversion of the W-Phase: Real-time Implementation and Extension to Low Magnitudes. *Seismological Research Letters*, *80*(5), 817–822. https://doi.org/10.1785/gssrl.80.5.817

Kanamori, H., & Rivera, L. (2008). Source inversion of Wphase: speeding up seismic tsunami warning. *Geophysical Journal International*, *175*(1), 222–238. https://doi.org/10.1111/j.1365-246X.2008.03887.x

Kawakatsu, H., & Yamamoto, M. (2015). 4.15 - Volcano Seismology. In G. Schubert (Ed.), *Treatise on Geophysics (Second Edition)* (pp. 389–419). Oxford: Elsevier. https://doi.org/10.1016/B978-0-444-53802-4.00081-6

National Research Institute for Earth Science and Disaster Resilience. (2019). NIED F-net [Data set]. National Research Institute for Earth Science and Disaster Resilience. https://doi.org/10.17598/NIED.0005

Sandanbata, O., Kanamori, H., Rivera, L., Zhan, Z., Watada, S., & Satake, K. (2021). Moment tensors of ring-faulting at active volcanoes: Insights into vertical-CLVD earthquakes at the Sierra Negra caldera, Galápagos islands. *Journal of Geophysical Research, [Solid Earth]*, *126*(6), e2021JB021693. https://doi.org/10.1029/2021jb021693

Sandanbata, O., Watada, S., Satake, K., Kanamori, H., Rivera, L., & Zhan, Z. (2022). Sub-decadal volcanic tsunamis due to submarine trapdoor faulting at Sumisu caldera in the Izu–Bonin arc. *Journal of Geophysical Research, [Solid Earth]*, *127*(9). https://doi.org/10.1029/2022jb024213

Sandanbata, O., Watada, S., Satake, K., Kanamori, H., & Rivera, L. (2023). Two volcanic tsunami events caused by trapdoor faulting at a submerged caldera near Curtis and Cheeseman islands in the kermadec arc. *Geophysical Research Letters*, *50*(7). https://doi.org/10.1029/2022gl101086

Takeuchi, H., & Saito, M. (1972). Seismic surface waves. *Methods in Computational Physics*, *11*, 217–295.